scientific reports

Check for updates

OPEN

A pair of primers facing at the double-strand break site enables to detect NHEJ-mediated indel mutations at a 1-bp resolution

Faryal Ijaz[1], Ryota Nakazato[1], Mitsutoshi Setou[2] & Koji Ikegami[1,2,3]✉

The introduction of small insertion/deletion (indel) mutations in the coding region of genes by the site-specific nucleases such as Cas9 allows researchers to obtain frameshift null mutants. Technically simple and costly reasonable genotyping methods are awaited to efficiently screen the frameshift null mutant candidates. Here, we developed a simple genotyping method called DST-PCR (Double-strand break Site-Targeted PCR) using "face-to-face" primers where the 3′ ends of forward and reverse primers face each other at the position between 3-bp and 4-bp upstream of the PAM sequence, which is generally the Cas9-mediated double-strand break site. Generated amplicons are directly subjected to TBE-High-Resolution PAGE, which contains a high concentration of bis-acrylamide, for mutant clones detection with 1-bp resolution. We present actual cases of screening of CRISPR/Cas9-engineered knockout (KO) cells for six genes, where we screen indels to obtain potential KO cell clones utilizing our approach. This method allowed us to detect 1-bp to 2-bp insertion and 1-bp to 4-bp deletion in one or both alleles of mutant cell clones. In addition, this technique also allowed the identification of heterozygous and homozygous biallelic functional KO candidates. Thus, DST-PCR is a simple and fast method to screen KO candidates generated by the CRISPR/Cas9 system before the final selection of clones with sequencing.

A prokaryotic RNA-mediated adaptive immune system known as clustered regularly interspaced short palindromic repeats (CRISPR)/CRISPR-associated protein 9 (Cas9) system has been developed into a revolutionary genome-editing technology[1]. The Cas9 nuclease combined with a short single-guide RNA (sgRNA) allows researchers to create site-specific double-strand breaks (DSBs)[2–4]. These DSBs are predominantly repaired by error-prone non-homologous end-joining (NHEJ) pathway often producing mutations of small nucleotide substitutions or insertion/deletion (indel) at the targeted sequence[5]. These indels are of interest to researchers to acquire frameshift null mutants for gene functional studies[6].

One of the major challenges to perform screening of knockout (KO) clones that possess CRISPR/Cas9-induced frameshift mutations is the need for simple and cost-effective strategies that do not require special equipment and are available in standard laboratories and institutes. Western blot analyses can be chosen for screening if reliable antibodies are available and the samples are cell lines. However, in many cases, genotyping with genomic DNA is required in cases where reliable antibodies are not available or the samples are not cell lines, e.g. animals. In these cases, initial screening is important to choose "best possible" candidates before sequencing.

The T7E1/Surveyor assays[7,8] are broadly used for detecting modified genes. They can detect heteroduplexes formed by the hybridization of wild-type and mutated DNA strands or two differently mutated DNA strands[9]. A weak point of the technique is that it cannot differentiate homozygous biallelic mutants from wild-type nor heterozygous biallelic mutants from heterozygous monoallelic mutants. In addition, this technique does not provide information about types of mutations as well as the number of indels, which hampers researchers to screen out indels of nucleotides of multiples of three. Another commonly used strategy for genotyping is CRISPR/Cas9-derived RNA-guided engineered endonucleases in Restriction fragment length polymorphism analysis

[1]Department of Anatomy and Developmental Biology, Graduate School of Biomedical and Health Sciences, Hiroshima University, 1-2-3 Kasumi, Minami-Ku, Hiroshima 734-8553, Japan. [2]Department of Cellular and Molecular Anatomy and International Mass Imaging Center, Hamamatsu University School of Medicine, Hamamatsu 431-3192, Japan. [3]JST, PRESTO, 4-1-8 Honcho, Kawaguchi, Saitama 332-0012, Japan. ✉email: k-ikegami@hiroshima-u.ac.jp

(RGEN-RFLP) analysis[10]. Unlike T7E1/Surveyor assay, it can detect homozygous biallelic mutants. This assay, however, still cannot provide information about the presence or absence of frameshift mutations.

Heteroduplex Mobility Assay (HMA) can also distinguish between the heteroduplexes and homoduplexes DNA in native PAGE but indels smaller than 3 bp in size can be missed[11,12]. Improved versions of the HMA called improved heteroduplex analysis (iHDA)[13] and Probe-Induced HMA (PRIMA)[14] use DNA probes to detect 1-bp pair indels after gene editing. Though these techniques can detect a wide range of indels, they does involve multiple steps. For instance, iHDA requires 200-bp probe for mutation detection where the probe needs to be synthesized through a two-step PCR or cloning[13]. Alternatively, probes can be purchased to save time but the fee for a 200-nucleotide oligo is relatively expensive. PRIMA solves this problem by making use of shorter probes; however, it requires additional PCR step before hybridization with the probes[14]. With additional PCR step, there will also be the need of pre-testing of PCR products. Moreover, in some cases with PRIMA, additional optimization time may be needed to test multiple probes for the same target or modifying DNA fragment size in order to detect heteroduplex signals[14].

In this paper, we present a very simple one-step PCR-based assay, namely DSB Site-Targeted PCR (DST-PCR) coupled with Tris–borate-EDTA high concentration bis-acrylamide gel electrophoresis (TBE-PAGE) for screening indels introduced by CRISPR/Cas9 genome editing in cultured cells with the 1-bp resolution. We here show the general applicability and reproducibility of DST-PCR in actual cases of screening of potential KO clones for six genes.

Materials and methods

Cell culture. NIH/3T3 cells, a fibroblast cell line derived from the whole murine embryo, were purchased from American Type Culture Collection (ATCC CRL-1658). IMCD3 cells, inner medullary collecting duct cell line derived from mouse, were purchased from American Type Culture Collection (ATCC CRL-2123). NIH/3T3 cells were cultured in DMEM-High glucose (044–29,765, Wako, Japan) containing 10% fetal bovine serum (FBS) (26,140,079, Gibco). IMCD3 were cultured in DMEM / Ham's F-12 (048–29,785, Wako, Japan) containing 10% FBS. All cell lines were maintained in a humidified incubator at 37 °C supplied with 5% CO_2 in the air. Cells were induced for ciliogenesis with the following conditions: Confluent NIH/3T3 cells were cultured in DMEM-High Glucose with 1% FBS for 12 h. Confluent mIMCD-3 were cultured in serum-free DMEM/ Ham's F-12 medium for 12 h.

Construct design. To construct all-in-one expression plasmids for KO, a 20-bp target sequence was subcloned into U6-gRNA/CMV-Cas9-2A-GFP plasmid backbone (ATUM, CA, USA). The target sequences of guide RNA were selected using Broad Institute GPP sgRNA Designer (https://portals.broadinstitute.org/gpp/public/analysis-tools/sgrna-design). Target sequences used in this study are listed as follows.

mDync2h1: TATACATACGAGTACCAGGT;
mIft144: TAAGGATAATCTAACCAGTG;
mInpp5e:AGTGATCGTCACCAGCCAAG;
mArntl:TTGTCGTAGGATGTGACCGA;
mPkd1 (Exon11): CATCATGCTGTAAGCCAATG;
mPkd1 (Exon15): ATTACATGGACATTTGACAT;
mPkd2:CCAATGTGTACTACTACACT;

Generation of knockout cell lines. KO cell lines were generated with a CRISPR/CAS9-based genome editing technique as described in previous studies[15,16]. Cells were plated at a density of 2×10^4 per cm^2 and were transfected with all-in-one plasmid U6-gRNA/CMV-Cas9-2A-GFP using polyethylenimine (PEI)[17]. After 3 days of transfection, GFP positive cells were sorted using a FACS Aria2 SORP cell sorter (Becton Dickinson) and were plated in an appropriate culture medium containing 1% Penicillin/Streptomycin (168–23,191, Wako, Japan) in a 12-well plate. The cells were later expanded into a 10-cm dish. Then, the cells were collected and single cell-cloned into 96-well plates with the limiting dilution-culture method at 1 cell/well. Cells were allowed to grow for 1–2 weeks. For the selection of monocolonies, microscopic observations were made to monitor single-cell colony formation and confluency. Selected colonies were expanded into the duplicate of multi-well plates from which one culture was used to make frozen stocks for subsequent use and the other culture for screening by genotyping. To extract genomic DNA cells were first lysed in lysis buffer (50 mM Tris, pH 7.5, 100 mM EDTA, 1% SDS) containing Proteinase K (0.4 mg/mL) at 70 °C for 60 min. The volume of the lysis buffer was adjusted according to the confluency of cell clones in each well. Half a volume of absolute ethanol was added to the mixture. Then, genomic DNA was isolated using Favor Prep Blood Genomic DNA Extraction Mini Kit (FABGK001-2, Favorgen Biotech Corp) and used for screening of mutant clones by DST-PCR.

Genotyping of CRISPR mutants with DST-PCR. Primers were designed based on the following criteria: the 3' end of both forward and reverse primers faced each other at the position between 3-bp and 4-bp upstream of the PAM sequence. The primers were designed for a product size ranging from 39- to 41-bp. Smaller amplicons (< 40-bp) are preferable to detect 1-bp indels. The list of primers used for genotyping and estimated amplicon size are listed in Table 1. The PCR fragment was prepared with a normal PCR protocol using KOD-Plus-Neo DNA polymerase (KOD-401, Toyobo, Japan) or ExTaq DNA Polymerase (RR001, Takara, Japan), both of which had 3'–5' exonuclease activities. With ExTaq DNA polymerase PCR was performed as follows: 5 min at 94 °C; 35 cycles of 15 s at 94 °C, 30 s at annealing temperature optimized for each DST primer pair, 30 s at 72 °C and for final extension 5 min at 72 °C. With KOD-Plus-Neo DNA polymerase PCR was performed as follows:

Gene targeted	Primers name	Primer sequence (5'–3')	Amplicon size (bp)
Dync2h1	Dync2h1_4966S_type Fw	CAGTATACATACGAGTACCA	40 bp
	Dync2h1_4966S_type Rv	CTTCTACCAAAAGTCCTACC	
Ift144	Ift144_838S_G Fw	GACCATAAGGATAATCTAACCA	41 bp
	Ift144_838S_G Rv	GTCTGTGACAAGGCCACAC	
Inpp5e	Inpp5e739AS Fw	TGGAGTGATCGTCACCAGCC	39 bp
	Inpp5e739AS Rv	GCAGACCCCGGAGCCCCTT	
Arntl	Arntl_456S_Fw	TGTTTGTCGTAGGATGTGAC	40 bp
	Arntl_456S_Rv	ACAAAGAGGATCTTCCCTCG	
Pkd1	Pkd1_2129AS_G_Fw	CAGCATCATGCTGTAAGCCA	39 bp
	Pkd1_2129AS_G_Rv	TGCTCCCTGGTGACCTCAT	
Pkd1	PKD1_3719S_G_FW	ACAACATTACATGGACATTTGA	41 bp
	Pkd1_3719S_G_Rv	TACTGTGCCATCTCCCATG	
Pkd2	Pkd2_741S _G Fw	AGCTCCAATGTGTACTACTAC	40 bp
	Pkd2_741S _G Rv	GCTGTGACAGTGTCCGAGT	

Table 1. DST-PCR primers for screening.

Gene targeted	Primers name	Primer sequence (5'-3')
Dync2h1	Dync2h1_Ex32Seq Fw	CTGGAGCTTAAGCTGAAAGCAC
	Dync2h1_Ex32Seq Rv	CGCTCTGCCACTCTACTGGA
Ift144	Ift144_838S_Seq Fw	GACCATAAGGATAATCTAACCA
	Ift144_838S_Seq Rv	ACCACGTGAATACGGACAGG
Inpp5e	Inpp5e ex1 seq Fw	AAGTTGGAGCGAACCCTGTC
	Inpp5e ex1 seq Rv	ATAGCCCCTGGGTAGCTAGT
Arntl	Seq_Arntl_456S_Fw	GACCAGGCACACACAGTCAC
	Seq_Arntl_456S_Rv	TTCCAGTTGGGGAAAATACG
Pkd1	gRNA_Pkd1_2129AS_Seq_Fw	TACGCTGTTGCCCACTGTAG
	gRNA_Pkd1_2129AS_Seq_Rv	GACTCAGCCATGAGTGCCTT
Pkd1	Pkd1_3719S_Seq_Fw	TGCCCTCAACTGATGGTGTC
	Pkd1_3719S_Seq_Fw	TGACATGGGCCATAAGCTGG
Pkd2	Pkd2_741S _Seq Fw	GAGCCACCTTGCTACACATTTC
	Pkd2_741S _Seq Rv	GAAAGCACTTTCAGCGTTCTCC

Table 2. Sequencing primers.

2 min at 94 °C; 35 cycles of 10 s at 98 °C, 30 s at annealing temperature optimized for each DST primer pair, 30 s at 68 °C and for final extension 5 min at 68 °C. Of note, we optimized DST-PCR with maximally high primer annealing temperatures for greater stringency. Details of PCR conditions are provided in Supplementary Table 1.

Twelve to 15% polyacrylamide gels were prepared using a 40% (w/v) Acrylamide/Bis mixed solution containing 38% (w/v) Acrylamide and 2% (w/v) bis-Acrylamide for a monomer to crosslinker ratio of 19:1 (Wako, Japan, 013–25,675) in 1X Tris–Borate-EDTA (TBE) buffer. Ten µL of each genomic DNA sample was loaded into each well and 1X TBE Buffer was used for electrophoresis to ensure adequate buffering power during vertical electrophoresis. The gels were electrophoresed at room temperature for ~ 60 min at 200 V (BLOT POWER-BP-T8, Biocraft, Japan) and stained with Midori Green (Nippon Genetics, Japan). The time of electrophoresis may need to be adjusted to the electrophoresis apparatus used. A DNA size marker (Gene Ruler Ultra Low Range DNA Ladder, Thermo Scientific, SM1211) was used. Images were acquired with FAS-Digi LED Imaging System (Nippon Genetics, Japan). Finally, the exact mutations in the selected screened samples were identified by direct Sanger sequencing. The list of primers used for Sanger sequencing is listed in Table 2. In order to get best possible KO clones, the KO candidates that were screened on the gel were selected for sequencing based on healthy cell growth and morphology.

Interpretation of sequencing chromatograms. Sanger sequencing chromatograms were interpreted manually and the wild-type sequences and information about the DSB-targeting site and corresponding PAM sequence were used as reference points. For heterozygous clone two peaks of different colors (overlapping peaks) instead of just one showing both nucleotides simultaneously for alternative allele sequences followed by single peak sequences were present. These overlapping peaks commonly starts at the point of mutations right after single peak sequence. The double peak regions (overlapping peaks) were detected by scanning through the sequence chromatograms in SnapGene Viewer. In order to interpret double peak chromatograms, the single

peak region was used to align the sequencing results to the provided reference. The double peak region was then separated into allele 1 and alternative allele 2 sequences manually and aligned to each other.

Antibodies. The antibodies used in this study are as follows: Arl13b (mouse mAb N295B/66; ab136648; Abcam), Arl13b (rabbit pAb; 17,711–1-AP; Protein Tech), Alexa fluorophore-conjugated secondary antibodies (Thermo) for immunofluorescence microscopy.

Immunocytochemistry (ICC). Cultured cells were fixed with 4% paraformaldehyde (PFA, pH7.5) for 30 min at 37 °C. Cells were washed with PBS and were blocked and permeabilized with 5% normal goat serum containing 0.1% Triton X-100 in PBS for 1 h at room temperature followed by incubation with the primary antibodies for 24 h at 4 °C. After washing in PBS, cells were incubated for 1 h at room temperature with Alexa Fluor-conjugated t secondary antibodies and DAPI (1:1000; DOJINDO). Images were acquired using a confocal microscope (Olympus FV1000) equipped with an oil immersion lens (60X, NA 1.35).

Results

Concept and design of DST-PCR coupled with TBE-High-Resolution-PAGE. A key element of DST-PCR assay is the primers, which are sensitive to indels at the Cas9-mediated DSB. We designed "face-to-face" primers that annealed to sequences in the genomic DNA spanning the targeted Cas9 DSB site with both forward and reverse primers 3' ends facing each other at the position between 3-bp and 4-bp upstream of the PAM sequence (Fig. 1a). The face-to-face primers generate a small amplicon ranging in size from 39- to 41-bp. After amplification with DST-PCR, PCR products are directly subjected to TBE-high-resolution PAGE, which contains high concentration of bis-acrylamide, for mutant clones detection. The use of TBE-PAGE allows discriminating the size of indels with 1-bp resolution. Amplicons generated from mutant alleles that harbor insertion mutations will be detected as upper band shifts depending on the number of insertions (Fig. 1b). Similarly, amplicons generated from mutant alleles that harbor short deletion mutations will be detected as lower band shifts depending on the number of deletions. In contrast, target sequences with longer deletion mutations will not be amplified because of the inability of the primers to anneal to the target sequences, especially the failure of 3' end of primers resulting in no band on the gel (Fig. 1b). In addition, amplicons generated from compound heterozygous mutant alleles that harbor insertion and deletion mutations will be detected as upper and lower band shifts depending on the number and position of the mutations and sequences of the targeted region (Fig. 1b).

DST-PCR coupled with TBE-High-Resolution-PAGE can efficiently screen insertion mutations induced by CRISPR/Cas9 gene editing. To evaluate the DST-PCR method, we first generated the CRISPR/Cas9-mediated NIH/3T3-*Dync2h1*-KO cells using sgRNA targeting exon 32 of murine *Dync2h1* gene locus (Fig. 2a). Dync2h1 is one of two cytoplasmic dynein heavy chain proteins that is responsible for the generation and maintenance of primary cilia[18]. Distinguishable band patterns between control cells and mutant clones were obtained from TBE-high-resolution-PAGE after DST-PCR. Control bands were detected at 40-bp, while #7 clone showed a 2-bp upper band shift (* of Fig. 2b), indicating insertion of 2 nucleotides into the target region of the *Dync2h1* gene on at least one allele. In clones #3 and # 4, a 1-bp upper band shift was detected; clone #5 also provided a 2-bp upper band shift (Fig. 2b). Clones #1, #2, #6, and #8, which showed no band shift (Fig. 2b), were eliminated in this screening.

We next confirmed the insertion mutations found in the *Dync2h1*-KO #7 using Sanger sequencing (Fig. 2c). The start of overlapping peaks is shown as a black rectangle, from which the split nucleotide sequences were shown under the chromatogram (Fig. 2c). In clone #7, two nucleotides (TA) were inserted between −6 and −5 from the third nucleotide (G) of the PAM motif (AGG), hereafter called position 0, in one allele (Fig. 2c). In the other allele, a 1-bp deletion occurred at −7 from position 0 (Fig. 2c), which failed to be detected in PAGE (Fig. 2b). Both these mutations result in frameshift missense mutation leading to the heterozygous biallelic functional knockout of the *Dync2h1* gene. The visibility of 2-bp resolution on the high-resolution PAGE was also confirmed by running triplicates of the DST-PCR amplicons from clone #7 and wild-type control samples (Supplementary Fig. 1a). To confirm the loss of Dync2h1 protein in the selected clone #7, we examined whether the cells showed deficiency in primary cilia using an antibody against the primary cilium marker Arl13b. Compared to wild-type cells, cells of clone #7 showed fewer primary cilia with shortened length (Fig. 2d) confirming the generation of the *Dync2h1*-KO cell line.

We further analyzed other clones that showed upper-shifted bands. Clone #5, which exhibited 2-bp upper shift of band in PAGE, harbored the same mutations as clone #7 (Supplementary Fig. 1b). Both clones #3 and #4 had an allele with a 1-bp insertion of nucleotide A and G respectively at −6 from position 0 (Supplementary Fig. 1b), confirming the 1-bp insertion detected initially by DST-PCR (Fig. 2b). Clone #3 harbored the other allele with 24-bp deletion in-frame shift, i.e. sense deletion mutation, while clone #4 bore a 1-bp and a 4-bp deletions in other two alleles (Supplementary Fig. 1b).

In addition, we applied DST-PCR to screen mutations in the mIMCD3 cells that have undergone CRISPR/Cas9 gene editing at exon 9 of endogenous murine intraflagellar transport protein 144 (*Ift144*) gene locus using Ift144 sgRNA to generate *Ift144*-KO clones (Fig. 2e). Genomic DNA was extracted from mutant cells derived from single-cell clones and subjected to DST-PCR. We found a 1-bp upper band shift in clones #4 (* of Fig. 2f) compared to control cells (41-bp band) (Fig. 2f). Likewise, in clones #1, #2 and # 6, a 1-bp upper band shift was also detected; clone #5 exhibited a 2-bp upper band shift (Fig. 2f). Clones #3 which showed no band shift (Fig. 2f), and clones #1 and #5 with abnormal cell morphology were eliminated in this screening.

Sanger sequencing of the clone #4 showed that it was a heterozygous biallelic functional KO with a 1-bp (A) insertion (−6 from position 0) in one allele, and a 1-bp diminish by replacement of 2-bp nucleotides (CC) by a

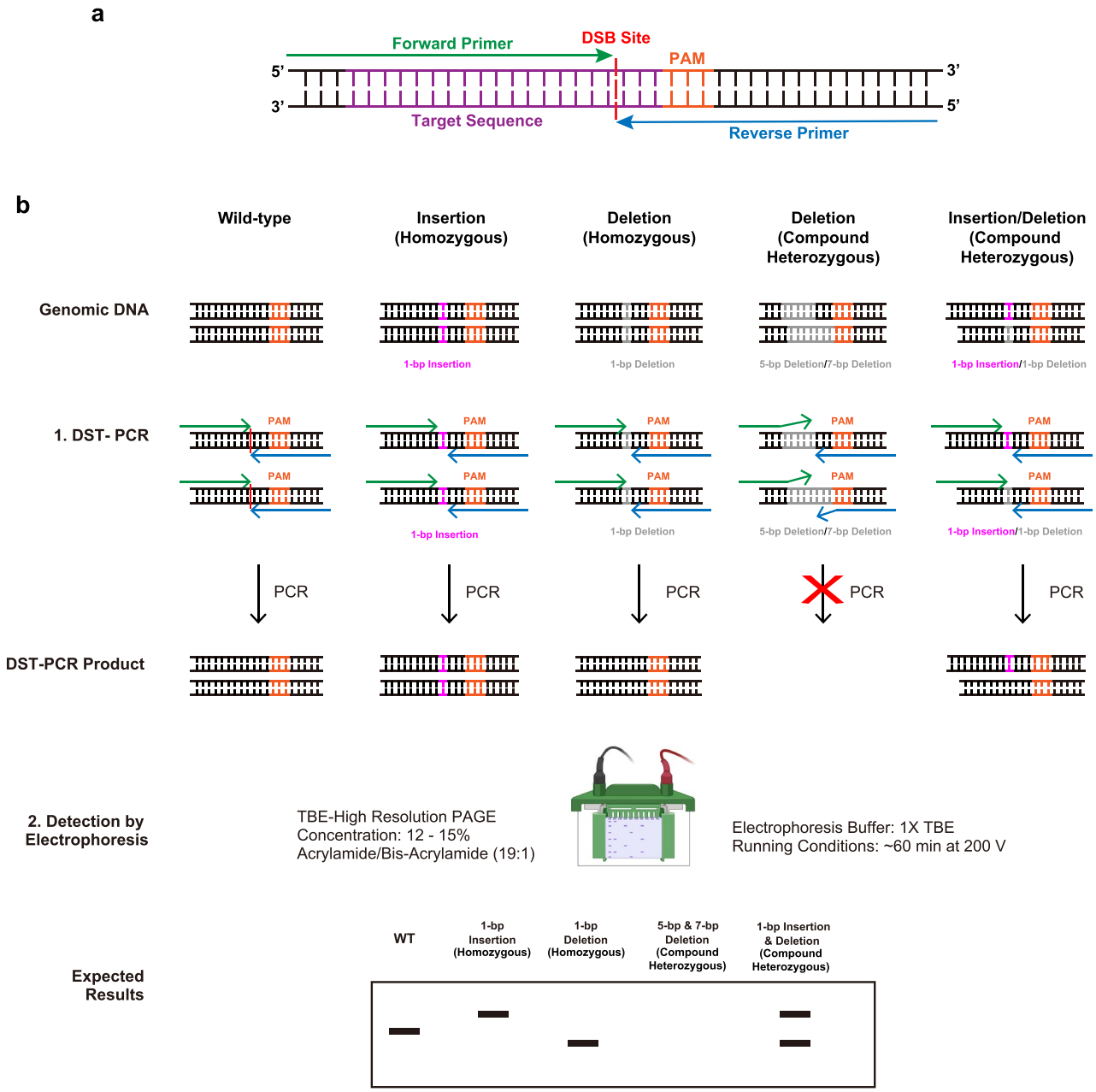

Figure 1. Overview of DST-PCR (DSB Site-Targeted PCR) (**a**) Principle of DST-PCR. Target sequences, PAM sequences, and double-strand break (DSB) are shown in magenta, orange, and red, respectively. Forward primer (green arrow) and reverse primer (blue arrow) face each other at the DSB site, i.e. between 3-bp and 4-bp upstream of the PAM sequence. (**b**) Overview of DST-PCR. 1. Principle of DST-PCR in distinguishing indels and wild-type sequences. Black lines represent genomic DNA from an allele of WT, 1-bp insertion (pink) mutant, and 1-bp deletion (grey) mutant. 2. Parameters for running TBE-PAGE and expected result of DST-PCR resolved by TBE-high-resolution-PAGE. Note that TBE-high-resolution-PAGE represents simplified pictures, it is possible that more than a single extra signal may be observed due to the nature of indels. Created in Adobe Illustrator CC V26.2.1 (https://adobe.com/products/illustrator) and adapted from "Protein Overexpression and Purification from Bacteria", by BioRender.com (2020). Retrieved from https://app.biorender.com/biorender-templates.

nucleotide A (−8 to −7 from position 0) in the other allele (Fig. 2g). Ift144 is a part of the IFT-A protein complex essential for anterograde transport in cilia and primary cilia formation[19,20]. The visibility of 1-bp resolution on high-resolution PAGE was also confirmed by running triplicates of the DST-PCR amplicons from clone #4 and wild-type control samples (Supplementary Fig. 1c). To confirm the loss of Ift144 protein in the KO cells, the primary cilium was visualized in clone #4 using an antibody against the primary cilium marker Arl13b. Compared to the wild-type cells, the clone #4 cells had no primary cilium (Fig. 2h), confirming the generation

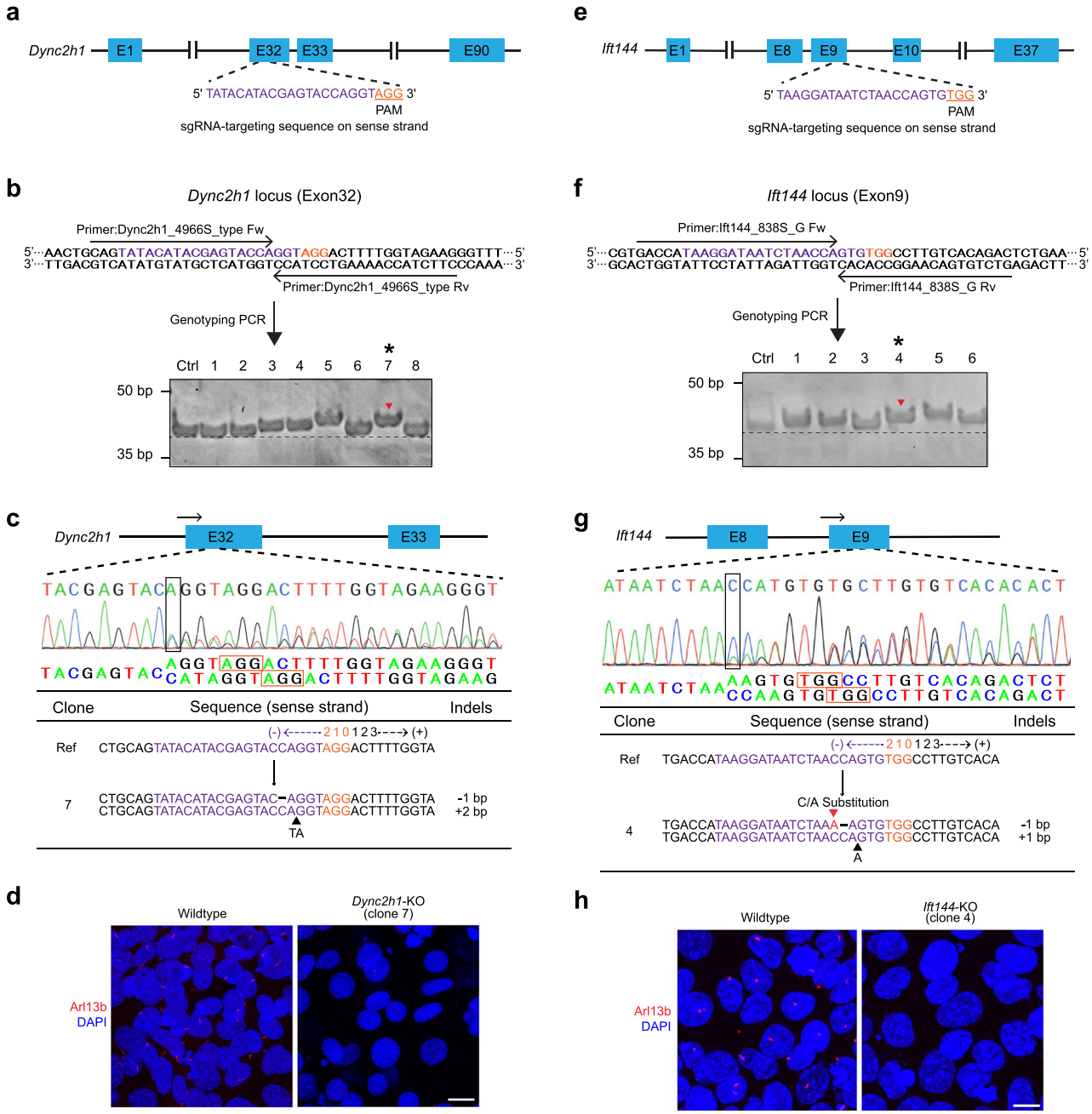

Figure 2. Detection of insertion mutations via DST-PCR (**a**) Scheme of the Dync2h1 guide RNA targeting exon 32 in the murine *Dync2h1* gene. (**b**) DST-PCR for screening mutations. Upper panel: The arrows indicate the locations of the DST-PCR primers (see Table 1). Bottom panel: TBE-high-resolution-PAGE of DST-PCR products. Lane Ctrl: PCR product (40-bp) amplified from the genomic DNA of wild-type unedited cells. Several clones including clone #7 (*) show fragments mobility upper shift (red arrowhead). (**c**) Sanger sequencing of the PCR products of clone #7 (* in panel b) around the PAM sequence (orange rectangle). Split sequences were shown under the spectrum. Start of split sequences are highlighted as black rectangle. The arrows indicate the locations of the sequencing primers (see Table 1). (**d**) Fluorescence microscopy images showing cells with primary cilium stained for the ciliary marker (Arl13b; red) and the nucleus (DAPI; blue) in wild-type and clone #7. Scale bar, 10 µm. (**e**) Scheme of the Ift144 guide RNA targeting exon 9 in the murine *Ift144* gene. (**f**) DST-PCR for screening mutations. Upper panel: The arrows indicate the locations of the DST-PCR primers (see Table 1). Bottom panel: TBE-high-resolution-PAGE of DST-PCR products. Lane Ctrl: PCR product (41-bp) amplified from the genomic DNA of wild-type unedited cells. Several clones including clone #4 (*) show fragments mobility upper shift (red arrowhead). (**g**) Sanger sequencing of the PCR products of clone #4 (* in panel **f**) around the PAM sequence (orange rectangle). Split sequences were shown under the spectrum. Start of split sequences are highlighted as black rectangle. The arrows indicate the locations of the sequencing primers (see Table 1). (**h**) Fluorescence microscopy images showing cells with primary cilium stained for the ciliary marker (Arl13b; red) and the nucleus (DAPI; blue) in wild-type and clone #4. Scale bar, 10 µm. The 20-bp sgRNA and 3-bp PAM sequences are highlighted in magenta and orange respectively. Wild-type sequence (Ref), base deletion (–), base insertion (▲), base substitution (▲, red). Original gels are presented in Supplementary Raw Data. Created in Adobe Illustrator CC V26.2.1 (https://adobe.com/products/illustrator).

of *Ift144*-KO cell line and the feasibility of our screening approach to detect small insertion induced by CRISPR/Cas9 system with 1-bp resolution.

The insertion mutations detected by DST-PCR in other clones with upper band shifts (Fig. 2f) were also further confirmed by sequencing. In both clones #2 and #6, a 1-bp (A) insertion occurred between −5 and −6 position in one allele (Supplementary Fig. 1d). Clone #2 also harbored an allele with a 3-bp in frameshift sense deletion mutation along with third allele with a 4-bp deletion, while clone #6 had second allele with a 1-bp deletion (Supplementary Fig. 1d). These results suggest that DST-PCR along with TBE-high-resolution-PAGE is able to identify insertion mutations in cell clones engineered through CRISPR/Cas9 editing.

DST-PCR coupled with TBE-High-Resolution-PAGE can detect deletion mutations induced by CRISPR/Cas9 gene editing. We further tested the efficiencies of DST-PCR along with TBE-high-resolution-PAGE to other genes. We attempted to generate KO mIMCD-3 cells of Inositol Polyphosphate-5-Phosphatase E (*Inpp5e*) gene that have undergone CRISPR/Cas9 gene editing using sgRNA sequences targeting exon 1 of murine *Inpp5e* locus as shown in Fig. 3a. Inpp5e compartmentalizes PIP in the primary cilium and regulates the primary cilium tip excision[15]. Target sequences were amplified using DST-PCR, and the amplicons were subjected to the TBE-high-resolution-PAGE, in which control bands were detected at 39-bp. Mutant clone #4 showed a 1-bp lower band shift at 38 bp as well as a 1-bp upper band shift at 40 bp (* of Fig. 3b). We selected only clone #4 in this case, since other clones #2, #3, and #5 showed abnormal shapes and clone #1 showed no band shift in PAGE (Fig. 3b). Sequencing results confirmed that clone 4 had a 1-bp deletion located at −5 from position 0 of the PAM motif (CCC) in one allele and a 1-bp (G) insertion (−6 from position 0) in the other allele (Fig. 3c). The visibility of 1-bp deletion mutation on high-resolution PAGE was also confirmed by running triplicates of the DST-PCR amplicons from clone #4 and wild-type control samples (Supplementary Fig. 2a).

We also analyzed NIH/3T3 cells clones lacking the aryl hydrocarbon receptor nuclear translocator-like (*Arntl*) gene. *Arntl* encodes Brain and muscle aryl hydrocarbon receptor nuclear translocator-like protein-1 (Bmal1) clock gene protein which is an essential component of the complex that regulates circadian rhythm in mammals[21]. We identified sgRNA sequences targeting exon 7 of the *Arntl* gene locus (Fig. 3d) and designed primers for screening as shown in Fig. 3e. After DST-PCR amplification, control bands were detected at 40-bp in the TBE-high-resolution-PAGE. Clone #3 exhibited lower band shifts of amplicons from both alleles with a 1-bp and a 4-bp faster migration (* of Fig. 3e). Clones #1, #4, #5, and #7 showed a single band with 1-bp upper band shift while clones #2 and #6 had a 1-bp upper and lower band shifts. Out of eight potential KO candidates, three clones (#1, #3, and #7) were selected for sequencing based on healthy cell growth and morphology (Fig. 3f, Supplementary Fig. 2b). Comparison of sequences near the *Arntl* sgRNA target site in clone #3 with the corresponding region in control cells showed that clone #3 had a 1-bp deletion located at −6 from position 0 of the PAM motif (GGG) in one allele and a 4-bp deletion (−9 to −6 from position 0) in the other allele (Fig. 3f). The visibility of 1-bp resolution of deletion mutations on high-resolution PAGE was also corroborated by running triplicates of the DST-PCR amplicons from clone #3 and wild-type control samples (Supplementary Fig. 2c). These findings demonstrate that DST-PCR is able to screen deletion mutations in cell clones engineered through CRISPR/Cas9 editing.

DST-PCR coupled with TBE-High-Resolution-PAGE can efficiently screen homozygous biallelic indel mutations induced by CRISPR/Cas9 gene editing. CRISPR/Cas9 system allows the efficient production of homozygous biallelic KO cells [22]. To assess the potential of DST-PCR to detect homozygous indel mutations, we attempted to induce DSB in exon 11 of endogenous murine polycystic kidney disease 1 gene (*Pkd1*) after CRISPR/Cas9 gene editing using Pkd1 sgRNA in mIMCD-3 cells (Fig. 4a). DST-PCR was performed using genomic DNA extracted from clones and control wild-type cells to amplify a 39-bp fragment corresponding to the target site in exon 11 of murine *Pkd1*. Amplicons from clone #1, #2, #3, and #5 were detected at the same size as control amplicon (40-bp) indicating the presence of wild-type Pkd1 allele in these cells and were eliminated in this screening (Fig. 4b). Clone #4 produced a single band with a 1-bp upper band shift compared to control cells. (*of Fig. 4b). Sequencing results confirmed that clone #1 had a 1-bp homozygous biallelic insertion located at −6 from position 0 of the PAM motif (AGG) (Fig. 4c).

As another example, homozygous indel mutations in exon 3 of endogenous murine polycystic kidney disease 2 gene (*Pkd2*) were screened after CRISPR/Cas9 gene editing using Pkd2 sgRNA in mIMCD3 cells (Fig. 4d). After DST-PCR, mutant clone #3 showed a 2-bp lower band shift (* of Fig. 4e) while the control band was detected at 40-bp (Fig. 4e). Comparison of indel sequences near the Pkd2 sgRNA target site in clone #3 with the corresponding region in control cells showed that clone #3 had a 2-bp homozygous deletion (−7 to −6 from position 0 of the PAM motif CGG) as shown in Fig. 4f. These data show that DST-PCR is able to screen homozygous biallelic indel mutations in cell clones engineered through CRISPR/Cas9 editing. Clones #1 (+2 and −1 band shift) and #2 (no band shift) were eliminated due to abnormal cell shapes and poor growth.

Discussion

In this study, we described DST-PCR as a simple method to screen KO candidates generated by the CRISPR/Cas9 system before the final selection of clones with sequencing. To demonstrate our method, we implemented it to identify insertions and deletions in genetically altered NIH/3T3 and mIMCD3 cell clones generated from CRISPR/Cas9 gene editing. Indels in one or both alleles were detected using DST-PCR followed by 12–15% TBE-PAGE of the amplicons with a high concentration of bis-acrylamide: 1-bp to 2-bp insertion mutations were detected in our hands. In the experiments for *Ift144* or *Dync2h1* KO, we detected amplicons only from one allele that harbors insertion mutations, while the homologous regions of the other alleles where a deletion or nucleotide substitution occurred were not amplified (Fig. 2b and f). The failure of amplification of target region of the allele

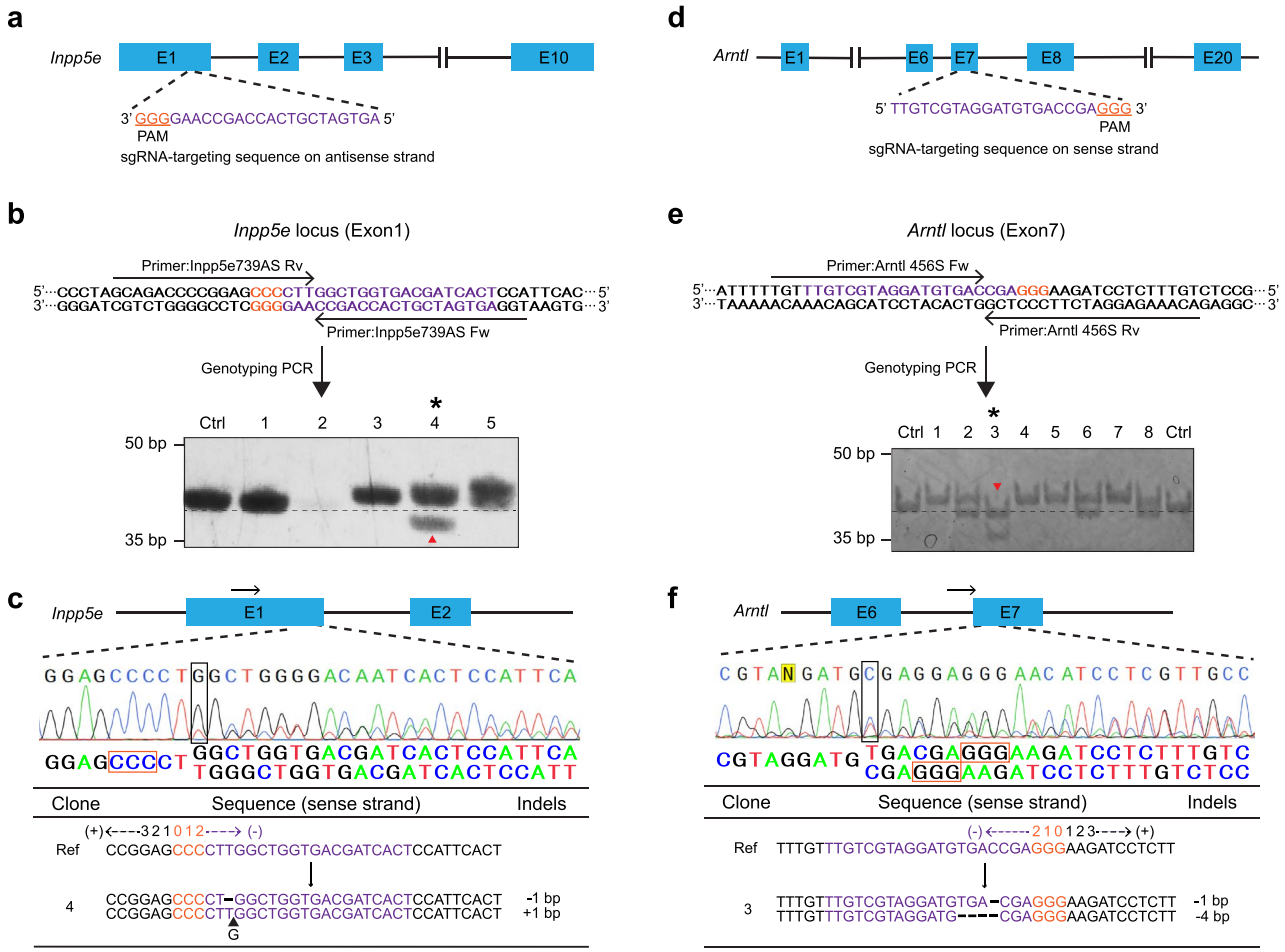

Figure 3. Detection of deletion mutations via DST-PCR (**a**) Scheme of the Inpp5e guide RNA targeting exon 1 in the murine *Inpp5e* gene. (**b**) DST-PCR for screening mutations. Upper panel: The arrows indicate the locations of the DST-PCR primers (see Table 1). Bottom panel: TBE-high-resolution-PAGE of DST-PCR products. Lane Ctrl: PCR product (39-bp) amplified from the genomic DNA of wild-type unedited cells. Clone #4 (*) exhibited a lower shifted band (red arrowhead) (**c**) Sanger sequencing of the PCR products of clone #4 (* in panel b) around the PAM sequence (orange rectangle). Split sequences were shown under the spectrum. Start of split sequences are highlighted as black rectangle. The arrows indicate the locations of the sequencing primers (see Table 1). (**d**) Scheme of the Arnt1 guide RNA targeting exon 7 in the murine *Arnt1* gene. (**e**) DST-PCR for screening mutations. Upper panel: The arrows indicate the locations of the DST-PCR primers (see Table 1). Bottom panel: TBE-high-resolution-PAGE of DST-PCR products. Lane Ctrl: PCR product (40-bp) amplified from the genomic DNA of wild-type unedited cells. Clone #2 (*) exhibited two lower shifted bands (red arrow head). (**f**) Sanger sequencing of the PCR products of clone #2 (* in panel e) around the PAM sequence (orange rectangle). Split sequences were shown under the spectrum. Start of split sequences are highlighted as black rectangle. The arrows indicate the locations of the sequencing primers (see Table 1). The 20-bp sgRNA and 3-bp PAM sequences are highlighted in magenta and orange respectively. Wild-type sequence (Ref), base deletion (–), base insertion (▲). Original gels are presented in Supplementary Raw Data. Created in Adobe Illustrator CC V26.2.1 (https://adobe.com/products/illustrator).

harboring deletion or substitution mutations could be attributed to allelic drop out during PCR and also the fact that extension of the annealing failure is allele and mismatch position-dependent[23–25]. We also observed that in some cases of genotyping, there were no bands on the gel (Supplementary Fig. 3) because the target regions were not amplified as a result of failure of primer annealing due to longer deletion mutations at the target site (Fig. 1b).The absence of amplification indicated the presence of deletion mutants harboring longer deletions.

Interestingly, with this approach, we were able to detect 1-bp to 4-bp deletion mutations (Fig. 3b and e). The potential mechanism that enables DST-PCR to detect these types of mutations is that the mismatched nucleotide at the primer 3' end was removed by the proofreading 3'–5' exonuclease activity of the high-fidelity DNA polymerases[26–28] such as ExTaq DNA polymerase and KOD-Plus-Neo DNA polymerase during polymerizing and hence restored the PCR amplification capacity in part or completely. This means that DNA polymerases

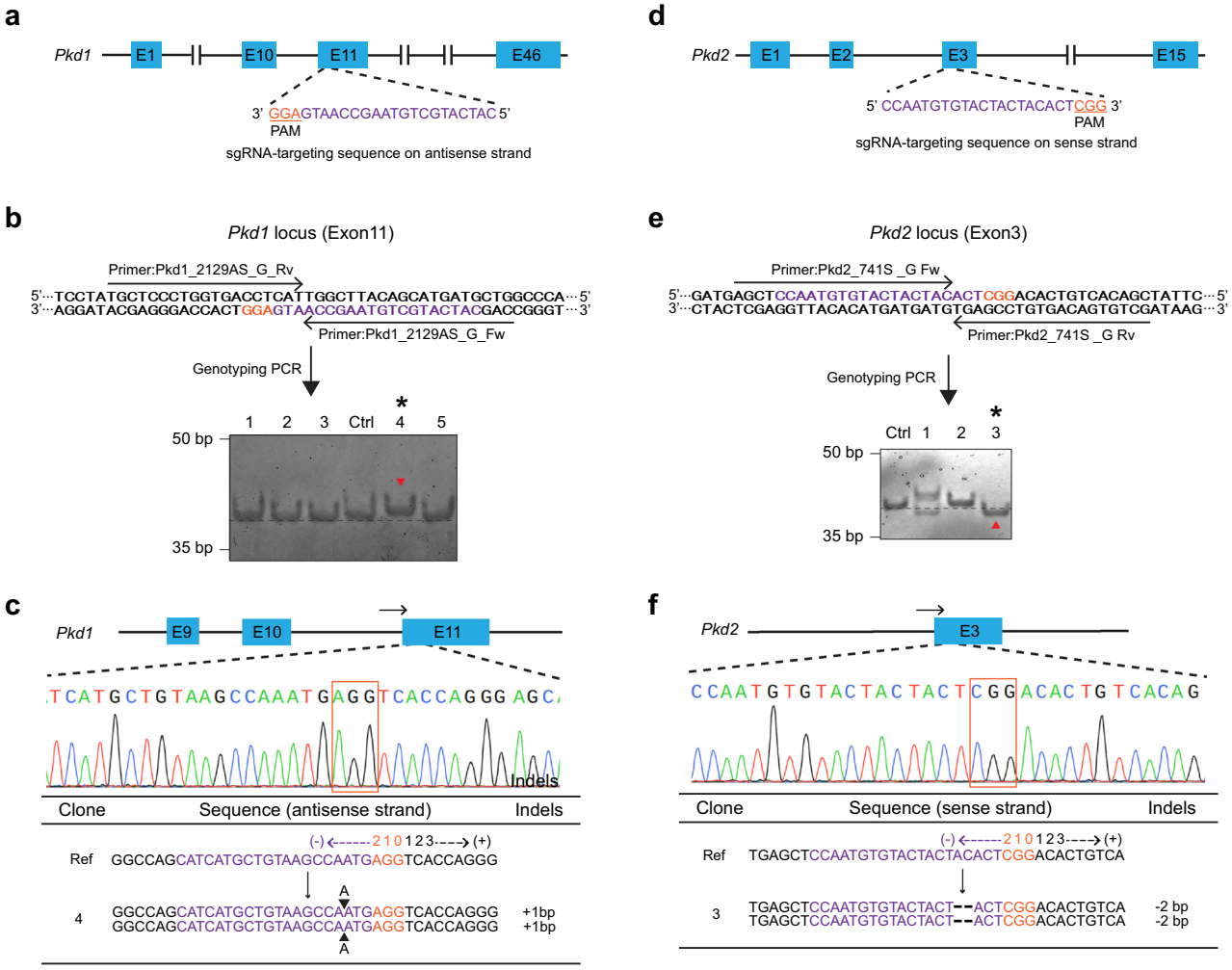

Figure 4. Detection of homozygous biallelic mutations via DST-PCR (**a**) Scheme of the Pkd1 guide RNA targeting exon 11 in the murine *Pkd1* gene. (**b**) DST-PCR for screening mutations. Upper panel: The arrows indicate the locations of the DST-PCR primers (see Table 1). Bottom panel: TBE-high-resolution-PAGE of DST-PCR products. Lane Ctrl: PCR product (39-bp) amplified from the genomic DNA of wild-type unedited cells. Clone #4 (*) showed a fragment mobility upper shift (red arrowhead). (**c**) Sanger sequencing of the PCR products of clone #4 (* in panel b) around the PAM sequence (orange rectangle). The arrows indicate the locations of the sequencing primers (see Table 1). (**d**) Scheme of the Pkd2 guide RNA targeting exon 3 in the murine *Pkd2* gene. (**e**) DST-PCR for screening mutations. Upper panel: The arrows indicate the locations of the DST-PCR primers (see Table 1). Bottom panel: TBE-high-resolution-PAGE of DST-PCR products derived. Lane Ctrl: PCR product (40-bp) amplified from the genomic DNA of wild-type unedited cells. Clone #3 (*) showed fragment mobility lower shift (red arrowhead). (**f**) Sanger sequencing of the PCR products of clone #3 (* in panel e) around the PAM sequence (orange rectangle). The arrows indicate the locations of the sequencing primers (see Table 1). The 20-bp sgRNA and 3-bp PAM sequences are highlighted in magenta and orange respectively. Wild-type sequence (Ref), base deletion (–), base insertion (▲). Original gels are presented in Supplementary Raw Data. Created in Adobe Illustrator CC V26.2.1 (https://adobe.com/products/illustrator).

play an important role in deciding the discrimination ability of DST-PCR with high-fidelity DNA polymerase, increasing its ability in distinguishing the indels. Yet, a downside of using proofreading DNA polymerases is that it could introduce a bias towards PCR priming efficiency[29].

The detection of deletion mutations can also occur independent of the 3'–5' exonuclease proofreading activity of the DNA polymerase at the primer 3' end mismatch, which depends on the sequence around the DSB site. The 1-bp deletion of a nucleotide C in one of the alleles of the target sequence of the *Arntl* gene changed the sequence from 5'-GACCGA-3' to 5'-GACGA-3' still enabling the DST-PCR screening primer pair to bind to DNA templates as the C/G complementarity was kept for the 3' end of the primers (Fig. 3e and f). Similarly, 2-bp deletion of nucleotides AC at the DSB site of the *Pkd2* gene was also detected (Fig. 4e). The sequence change from

5'-TACACT-3' to 5'-TACT-3' did not cause the mismatch between the primers and DNA templates (Fig. 4f). Both forward and reverse primers 3' end (TAC of forward, AGT of reverse) could anneal to the DNA templates with perfect complementarity at the DSB site leading to the amplification of the fragment.

Our approach overcomes several weak points of widely used commercially available genotyping assays such as T7E1/Surveyor. These assays do not provide information for base number of indels as well as types of mutations. DST-PCR was able to detect the number of bases of indels with 1-bp resolution (Supplementary Fig. 1c, Supplementary Fig. 2a and 2b, Supplementary Fig. 4d). Moreover, with the mismatch assays, a possibility of false-positive results remains[10,30]; which is not an issue with the DST-PCR approach. These assays may lead to inaccurate conclusions as they are unable to distinguish between monoallelic mutants and heterozygous biallelic mutants[10,31,32], resulting in failure of excluding monoallelic mutants. Our approach can strongly screen out heterozygous monoallelic mutants that possess an unedited wild-type allele by excluding clones that show migration of bands identical to the wild-type sample. In addition, the mismatch assays technically miss homozygous biallelic mutants[10,31,32]. Our approach can detect homozygous biallelic mutants (Fig. 4).

The other benefit of our approach is the simplicity. Previously developed methods such as T7E1/Surveyor, RGEN-RFLP, DNA melting analysis[33], and fluorescent PCR[31] require additional enzymes, denaturing and hybridization of PCR products, specific oligonucleotide probes, and/or special chemicals. Our DST-PCR approach is truly a simple PCR which does require neither additional steps, special enzymes, nor chemicals. DST-PCR can be performed in any standard laboratory using a regular thermal cycler and PAGE instrumentation. Results can be obtained rapidly with a ~ 6-h turnaround time including gel preparation, completion of PCR and resolving DST-PCR amplicons on TBE-high-resolution PAGE. As only positive clones screened through DST-PCR need to be confirmed, it could lower the cost for subsequent confirmation by Sanger sequencing.

Direct sequencing of PCR products without the need for cloning individual PCR fragments is compatible with our approach. Except the mutation is homozygous, direct Sanger sequencing of DNA from diploid organisms with heterozygous mutations generates two overlapping traces at the mutation start site. When clones screened through DST-PCR and TBE-high-resolution PAGE are selected for Sanger sequencing, the information obtained about base numbers of indels is also helpful for subsequent sequence data analysis. With this prior knowledge of where and how many nucleotides are inserted or deleted in at least one allele, two overlapping traces can be easily interpreted manually. We found that manual alignment of the overlapping peaks overcomes failure of sequence unmixing when using web application such as CRISPR-ID[34], which showed some limitations in accurately deciphering the complex sequencing peaks of the heterozygote samples.

We have designed DST-PCR to screen for indels in the region where the Cas9 preferentially cuts 3–4 bp upstream of the PAM sequence. Therefore, DST-PCR works very well for detecting fixed mutations ideally at a single nucleotide range from a DSB site (Fig. 1b). In addition to detecting fixed mutations, DST-PCR can give an idea about the indels broader nucleotide range at least for deletion mutations. For example, in case of longer deletions, there will be no amplification indicating KO-deletion mutants as we have shown in Supplementary Fig. 3. Thus, it is better to pay attention to not only what is amplified but also what is not amplified after DST-PCR. One of the limitations of our approach is that the DST-PCR can only detect mutations close to the PAM i.e. in the range of 3–6 bp upstream of PAM sequence, which are most frequent when using the CRISPR/Cas9 system, and not suitable to detect broader range of mutations for absolute quantification of gene-editing efficiencies. One way to widen the mutation detection range is to modify the screening primer pair design such that the 3' ends of both forward and reverse primers are designed to face 4-bp gaps on the DSB site. Eighteen base pairs primer size would be optimal for this modified design. Additionally, other suitable genotyping methods can also be applied for quantification purposes. Therefore, an appropriate genotyping method needs to be selected depending on the project requirements, cost, and time (Table 3). We designed DST-PCR to primarily function as a simple and fast screening method to get best possible candidates of knock-out clones, therefore, it is not necessary to detect absolute range of mutations to pick up all mutant clones in screening. Selecting several highly probable candidate clones are enough for screening. When clones that were suitable for DST-PCR are selected, our methods can be applied to genotyping as well, especially for animal experiments.

In addition, as our approach is based on PCR, there is a possibility of allele drop-out[23–25] and the PCR step may be biased towards the more abundant template and a small number of mutated sequence may not be detected[29,35], for example in case of compound heterozygotes where one mutated template is more abundant than the other mutated template. Therefore, it is necessary to sequence the target region to confirm the outcome of genome editing. Furthermore, there may be limitations to designing primers for genotyping in high GC content regions or highly repetitive sequences in the target region[36–38]. Finally, there might be nonspecific signals that are shared among the lanes in WT and mutant clones. However, this problem can be solved by carefully designing and optimizing the PCR stringency conditions to avoid non-specific bands.

In summary, we have established a very simple, PCR-based genotyping DST-PCR method to screen for indels in cell lines generated by CRISPR/Cas9 system. Here we showed the actual cases of screening where we succeeded in acquiring multiple KO clones using DST-PCR for six genes. Our data demonstrate that this approach can identify both on-target insertions and deletions irrespective of the zygosity of the mutants in cell lines, supporting the general applicability and reproducibility of DST-PCR. It will allow researchers to screen for mutant clones without the need for special enzymes or devices in the lab and can be implemented with standard molecular biology equipment. While we did not yet try to genotype transgenic cell lines generated by zinc-finger nucleases (ZFN)[39] and transcription activator-like nuclease (TALEN)[40], this method will likely be applicable, as DNA modifications through NHEJ with these systems is fundamentally the same as with the CRISPR/Cas9 system.

Methods	Type of mutations preferentially detected	Determination of mutation type	Advantages	Disadvantages
Mismatch cleavage assay	small indels	No	Commercialy available Able to detect SNPs	Requires special chemicals or devices Time consuming enzymatic reactions
NGS	All	If insertion or deletion	High throughput	Very expensive (> 500 US$ per assay)
DST-PCR	small indels	If insertion or deletion	Simple One step PCR process for screening 1-bp resolution for mutation detection	Not suitable for mutation quantification because of limited mutation detection range (3–6 bp upstream of PAM) Misses substitutions
HMA	small indels	No	2–3 bp resolution for mutation detection	Requires additional PCR step to determine zygosity
PRIMA	small indels	If insertion or deletion	Simple Able to detect SNPs 1-bp resolution for mutation detection	Requires preamplification and pretesting before probe hybridization Additional optimization steps may be needed to test multiple probes for the same target
iHDA	small indels	If insertion or deletion	1-bp resolution for mutation detection	Expensive and time consuming when 200 bp probe needs to be purchased or made in-house through cloning or two-step PCR process Requires preamplification and pretesting before probe hybridization

Table 3. Comparison of DST-PCR with other methods.

Data availability

The datasets generated during the current study are available in the NCBI BioProject database (https://www.ncbi.nlm.nih.gov/bioproject/PRJNA850849).

Received: 7 February 2022; Accepted: 29 June 2022
Published online: 08 July 2022

References

1. Jinek, M. *et al.* A programmable dual-RNA–guided DNA endonuclease in adaptive bacterial immunity. *Science* **337**, 816–821 (2012).
2. Cong, L. *et al.* Multiplex genome engineering using CRISPR/Cas systems. *Science* **339**, 819–823 (2013).
3. Mali, P. *et al.* RNA-guided human genome engineering via Cas9. *Science* **339**, 823–826 (2013).
4. Anders, C., Niewoehner, O., Duerst, A. & Jinek, M. Structural basis of PAM-dependent target DNA recognition by the Cas9 endonuclease. *Nature* **513**, 569–573 (2014).
5. Lieber, M. R., Ma, Y., Pannicke, U. & Schwarz, K. Mechanism and regulation of human non-homologous DNA end-joining. *Nat. Rev. Mol. Cell Biol.* **4**, 12–720 (2003).
6. Hu, W. *et al.* RNA-directed gene editing specifically eradicates latent and prevents new HIV-1 infection. *Proc. Natl. Acad. Sci. U.S.A.* **111**, 11461–11466 (2014).
7. Mashal, R. D., Koontz, J. & Sklar, J. Detection of mutations by cleavage of DNA heteroduplexes with bacteriophage resolvases. *Nat. Genet.* **9**, 177–183 (1995).
8. Qiu, P. *et al.* Mutation detection using Surveyor™ nuclease. *Biotechniques* **36**, 702–707 (2004).
9. Vouillot, L., Thélie, A. & Pollet, N. Comparison of T7E1 and surveyor mismatch cleavage assays to detect mutations triggered by engineered nucleases. *G3-Genes Genom. Genet.* **5**, 407–415 (2015).
10. Kim, J. M., Kim, D., Kim, S. & Kim, J. S. Genotyping with CRISPR-Cas-derived RNA-guided endonucleases. *Nat. Commun.* **5**, 1–8 (2014).
11. Bhattacharyya, A. & Lilley, D. M. The contrasting structures of mismatched DNA sequences containing looped-out bases (bulges) and multiple mismatches (bubbles). *Nucleic Acids Res.* **17**, 6821–6840 (1989).
12. Kumeda, Y. & Asao, T. Heteroduplex panel analysis, a novel method for genetic identification of Aspergillus section Flavi strains. *Appl. Environ. Microbiol.* **67**, 4084–4090 (2001).
13. Fan, J., Xia, Y. & Wang, G. L. An improved heteroduplex analysis for rapid genotyping of SNPs and single base pair indels. *Biotechniques* **67**, 6–10 (2019).
14. Kakui, H., Yamazaki, M. & Shimizu, K. K. PRIMA: a rapid and cost-effective genotyping method to detect single-nucleotide differences using probe-induced heteroduplexes. *Sci. Rep.* **11**, 1–10 (2021).
15. Phua, S. C. *et al.* Dynamic remodeling of membrane composition drives cell cycle through primary cilia excision. *Cell* **168**, 264–279 (2017).
16. Ijaz, F. & Ikegami, K. Knock-in of labeled proteins into 5'UTR enables highly efficient generation of stable cell lines. *Cell Struct. Funct.* **46**, 21–35 (2021).
17. Longo, P. A., Kavran, J. M., Kim, M. S. & Leahy, D. J. Transient mammalian cell transfection with polyethylenimine PEI. *Meth. Enzymol.* **529**, 227–240 (2013).
18. Mikami, A. *et al.* Molecular structure of cytoplasmic dynein 2 and its distribution in neuronal and ciliated cells. *J. Cell Sci.* **115**, 4801–4808 (2002).
19. Liem, K. F. Jr. *et al.* The IFT-A complex regulates Shh signaling through cilia structure and membrane protein trafficking. *J. Cell Biol.* **197**, 89–800 (2012).
20. Basten, S. G. & Giles, R. H. Functional aspects of primary cilia in signaling, cell cycle and tumorigenesis. *Cilia* **2**, 1–23 (2013).
21. Bunger, M. K. *et al.* Mop3 is an essential component of the master circadian pacemaker in mammals. *Cell* **103**, 1009–1017 (2000).
22. Sato, M. *et al.* The combinational use of CRISPR/Cas9-based gene editing and targeted toxin technology enables efficient biallelic knockout of the α-1, 3-galactosyltransferase gene in porcine embryonic fibroblasts. *Xenotransplantation* **21**, 291–300 (2014).
23. Martins, E. M. *et al.* Consequences of primer binding-sites polymorphisms on genotyping practice. *Open J. Genet.* **1**, 15–17 (2011).
24. Stevens, A. J., Taylor, M. G., Pearce, F. G. & Kennedy, M. A. Allelic dropout during polymerase chain reaction due to G-quadruplex structures and DNA methylation is widespread at imprinted human loci. *G3-Genes Genom. Genet.* **7**, 1019–1025 (2017).

25. Shestak, A. G., Bukaeva, A. A., Saber, S. & Zaklyazminskaya, E. V. Allelic dropout is a common phenomenon that reduces the diagnostic yield of PCR-based sequencing of targeted gene panels. *Front. Genet.* **12**, 620337 (2021).
26. Gohl, D. M. *et al.* Systematic improvement of amplicon marker gene methods for increased accuracy in microbiome studies. *Nat. Biotechnol.* **34**, 942–949 (2016).
27. Li, B., Ren, N., Yang, L., Liu, J. & Huang, Q. A qPCR method for genome editing efficiency determination and single-cell clone screening in human cells. *Sci. Rep.* **9**, 1–15 (2019).
28. Gohl, D. M. *et al.* Dissecting and tuning primer editing by proofreading polymerases. *Nucleic Acids Res.* **49**, e87 (2021).
29. Pan, W. *et al.* DNA polymerase preference determines PCR priming efficiency. *BMC Biotechnol.* **14**, 1–17 (2014).
30. Zischewski, J., Fischer, R. & Bortesi, L. Detection of on-target and off-target mutations generated by CRISPR/Cas9 and other sequence-specific nucleases. *Biotechnol. Adv.* **35**, 95–104 (2017).
31. Kim, H. *et al.* Surrogate reporters for enrichment of cells with nuclease-induced mutations. *Nat. Methods* **8**, 941–943 (2011).
32. Sentmanat, M. F., Peters, S. T., Florian, C. P., Connelly, J. P. & Pruett-Miller, S. M. A survey of validation strategies for CRISPR-Cas9 editing. *Sci. Rep.* **8**, 1–8 (2018).
33. Dahlem, T. J. *et al.* Simple methods for generating and detecting locus-specific mutations induced with TALENs in the zebrafish genome. *PLoS Genet.* **8**, e1002861 (2012).
34. Dehairs, J., Talebi, A., Cherifi, Y. & Swinnen, J. V. CRISP-ID: Decoding CRISPR mediated indels by Sanger sequencing. *Sci. Rep.* **6**, 1–5 (2016).
35. Polz, M. F. & Cavanaugh, C. M. Bias in template-to-product ratios in multitemplate PCR. *Appl. Environ. Microbiol.* **64**, 3724–3730 (1998).
36. Sahdev, S., Saini, S., Tiwari, P., Saxena, S. & Saini, K. S. Amplification of GC-rich genes by following a combination strategy of primer design, enhancers and modified PCR cycle conditions. *Mol. Cell. Probes* **21**, 303–307 (2007).
37. Kumar, A. & Kaur, J. Primer based approach for PCR amplification of high GC content gene: Mycobacterium gene as a model. *Mol. Biol. Int.* **2014**, 937308 (2014).
38. Hommelsheim, C. M., Frantzeskakis, L., Huang, M. & Ülker, B. PCR amplification of repetitive DNA: A limitation to genome editing technologies and many other applications. *Sci. Rep.* **4**, 1–13 (2014).
39. Ramirez, C. L. *et al.* Unexpected failure rates for modular assembly of engineered zinc fingers. *Nat. Methods* **5**, 374–375 (2008).
40. Joung, J. K. & Sander, J. D. TALENs: a widely applicable technology for targeted genome editing. *Nat. Rev. Mol. Cell Biol.* **14**, 49–55 (2013).

Acknowledgements

This work was supported in part by Japan Society for Promotion of Science Grants-in-Aid for Scientific Research Activity Start-up 19K23728 and for Early-Career Scientists 21K15088 (to F.I.), Japan Society for Promotion of Science Grant-in-Aid for Early-Career Scientists 20K15792 (to R.N.), and Japan Society for Promotion of Science Grant-in-Aids for Scientific Research on Innovative Areas 15H01207 and for Scientific Research (C) 21K06172 and Japan Science and Technology Agency, Precursory Research for Embryonic Science and Technology JPMJPR17H1 (to K.I.). A part of this work was carried out at the Natural Science Center for Basic Research and Development, Hiroshima University, and at Advanced Research Facilities and Services, Preeminent Medical Photonics Education and Research Center, Hamamatsu University School of Medicine. We thank Kiyoshi Shibata, Madoka Hamada, Mimoko Katoh, and Yoko Hayashi for their technical assistance.

Author contributions

K.I. designed research; F.I., R.N., and K.I. performed experiments and acquired the data; F.I., R.N., M.S., and K.I. analyzed the data; F.I., R.N., and K.I. wrote the paper; all authors discussed the results and commented on the manuscript.

Competing interests

The authors declare no competing interests.

Additional information

Supplementary Information The online version contains supplementary material available at https://doi.org/10.1038/s41598-022-15776-5.

Correspondence and requests for materials should be addressed to K.I.

Reprints and permissions information is available at www.nature.com/reprints.

Publisher's note Springer Nature remains neutral with regard to jurisdictional claims in published maps and institutional affiliations.

Open Access This article is licensed under a Creative Commons Attribution 4.0 International License, which permits use, sharing, adaptation, distribution and reproduction in any medium or format, as long as you give appropriate credit to the original author(s) and the source, provide a link to the Creative Commons licence, and indicate if changes were made. The images or other third party material in this article are included in the article's Creative Commons licence, unless indicated otherwise in a credit line to the material. If material is not included in the article's Creative Commons licence and your intended use is not permitted by statutory regulation or exceeds the permitted use, you will need to obtain permission directly from the copyright holder. To view a copy of this licence, visit http://creativecommons.org/licenses/by/4.0/.

© The Author(s) 2022